RESEARCH ARTICLE | JANUARY 21 2016

Wind tunnel investigation on the two- and three-blade Savonius rotor with central shaft at different gap ratio

Liu Chen; Jian Chen; Hongtao Xu; Hongxing Yang; Changwen Ye; Di Liu

J. Renewable Sustainable Energy 8, 013303 (2016)
https://doi.org/10.1063/1.4940434

Wind tunnel investigation on the two- and three-blade Savonius rotor with central shaft at different gap ratio

Liu Chen,[1] Jian Chen,[1,a)] Hongtao Xu,[1] Hongxing Yang,[2] Changwen Ye,[3] and Di Liu[2]
[1]*School of Energy and Power Engineering, University of Shanghai for Science and Technology, Shanghai 200093, People's Republic of China*
[2]*Renewable Energy Research Group (RERG), The Hong Kong Polytechnic University, Kowloon, Hong Kong, China*
[3]*State Key Laboratory of Geohazard Prevention and Geoenvironment Protection, Chengdu University of Technology, Chengdu 610059, People's Republic of China*

(Received 3 October 2015; accepted 8 January 2016; published online 21 January 2016)

The Savonius rotor seems to be a promising wind turbine as it not only has the simplest and cheapest design but also is capable of yielding a higher annual energy output at low wind speed than the Darrieus rotor. Moreover, the Savonius rotor can also be used in ventilation systems, for local electricity production, as the start-up device for the Darrieus rotor, and small hydrokinetic turbines operating at low velocity. As a two-blade Savonius rotor suffers from negative average static torque coefficient (AC_{TS}) at some azimuth angles and large-amplitude variation of AC_{TS}, several studies have been conducted in recent years to improve AC_{TS}. The three-blade rotor seems to be a potential candidate for AC_{TS} improvement. However, less research has been done on three-blade rotors with a 180° arc and central shaft at different gap ratios (GRs) for different wind speeds. Therefore, the focus of the present work is to compare the two- and three-blade rotor in terms of AC_{TS} and power coefficient (C_P) through a wind tunnel experiment. Results show that the wind speed had a small effect on AC_{TS}. However, negative azimuth angle range is narrowed and the negative azimuth angle range is moved upward as GR increased. Hence, the Savonius rotor with three blades could not only eliminate the negative range of AC_{TS} but also smooth AC_{TS} curves. In terms of the C_P, the maximum power coefficient of the two-blade configuration was approximately 1.5 times that of the three-blade configuration. The 1/6 GR test data exhibited the attainment of super performance for all wind speed and blade number. © *2016 AIP Publishing LLC*.
[http://dx.doi.org/10.1063/1.4940434]

I. INTRODUCTION

The vertical axis wind turbine (VAWT) has been reported as a potential renewable device in the field of construction.[1] There are two types of VAWTs: the Savonius rotor and the Darrieus rotor. The Darrieus rotor is superior to the Savonius rotor in terms of power efficiency. However, the Darrieus rotor features a very small starting torque and may fail to accelerate beyond the "dead band" even when it does begin to run.[2] This drawback has limited the utilization of Darrieus rotor in buildings area to a great extent. Recent researches showed that the Savonius rotor can have a high annual energy output at a relatively low wind speed making these micro wind turbines suitable for application on urban terrain.[3] From this point, the Savonius rotor seems to be a promising wind turbine as it not only has the simplest and cheapest design but also is capable of producing a higher annual energy output at low wind speed than the Darrieus rotor.[4] Moreover, the Savonius rotor can also be used in the ventilation

a)Email: 09900589r@connect.polyu.hk

system, for local electricity production,[5] as a start-up device[6] for the Darrieus rotor and in small hydrokinetic turbines operating at low velocity.[7]

Numerous numerical and experimental investigations have been conducted on the Savonius rotor recently, with the focus mainly on the blade profile,[8–11] the multi-stage,[12–15] the blade number,[16] the aspect ratio,[17,18] the gap ratio (GR),[19] and the argument (block) device.[4] From these researches, it is known that the optimization of the blade profile will directly increase the C_P of the rotor;[5] that multi-stage designs have been investigated mainly to unify the static torque coefficient (C_{TS}) or eliminate the negative C_{TS} range;[20] and that secondary design parameters, such as the aspect ratio and GR, are highly dependent on the blade profile design and the blade number. Among the aforementioned research topics, the literature review revealed that very few published papers have investigated the effect of blade number. The most well-known paper about the blade number was published by Blackwell *et al.*[21] in 1977, who conducted a comprehensive experimental investigation on one-stage two- and three-bladed Savonius rotors without shaft at wind speeds of 7 m/s and 14 m/s, wherein the blade profile of the three-blade rotor was built with a 150° arc, the arc of the blade profile was about 20° and 10° on the outer and inner edges, respectively, and the GR ranged from 0 to 0.2 and the height ratio from 1 to 1.5. The sweep areas of the tested rotors are different from each other. In 2005, Islam *et al.*[22] studied the static characteristics of two-, three-, and four-bladed Savonius rotors without shaft when GR was 0.2. Biswas *et al.*[23] inspected the effects of overlap and blockage on a three-blade Savonius rotor. Morshed *et al.*[24] conducted an experimental and numerical investigation on three different three-blade Savonius rotors with 0, 0.12, and 0.26 overlap ratios and without central shaft, respectively. Hayashi *et al.*[25] tested and compared a one-stage three-blade Savonius rotor with a three-stage three-blade Savonius rotor. In fact, researches done by Biswas and Hayashi focused on the overlap effect and the stage effect, respectively.

Different from previous researches, we laid the focus on two- and three-blade Savonius rotors with the same sweep area for all rotors and a shaft at the center of the rotor. The use of center shaft can improve the stability of the whole system. GR values studied in this paper were 0, 1/3, and 2/3. However, the definition of this GR (with shaft) is different from that of the rotor without shaft. This difference will be discussed in Section II C. The blade profile of a three-blade rotor was constructed with a 180° arc, instead of a 150° arc,[21] for the purpose of easy manufacturing and fabrication. Besides, considering the application in building area, a series of tests were also conducted at relatively low wind speeds. Hence, this paper studied the impact of blade number, wind speed and GR on C_P and C_{TS}.

II. EXPERIMENTAL INSTRUMENTATION AND TESTING MODELS

A. Wind tunnel

The wind tunnel shown in Figure 1 is a low speed open-circuit environmental wind tunnel (EWT) consisting of four sections (i.e., contraction section, test section, developed section, and diffuser section). In this wind tunnel, a honeycomb flow straighter is placed at the upstream of the contraction section to coordinate the speed of the oncoming wind and reduce the turbulence intensity; the air flow is then accelerated in the contraction section to gain a desired speed for the test section; and the test section is a square cross section (1050 mm × 1050 mm) and have

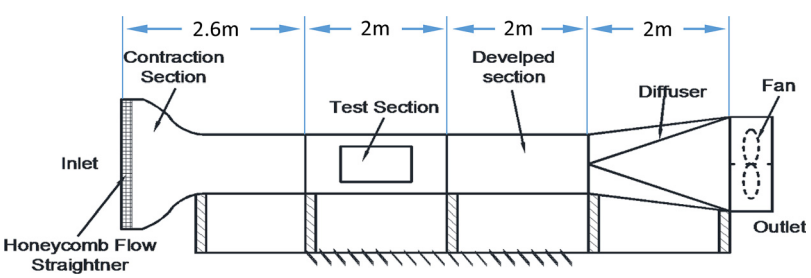

FIG. 1. Wind tunnel.

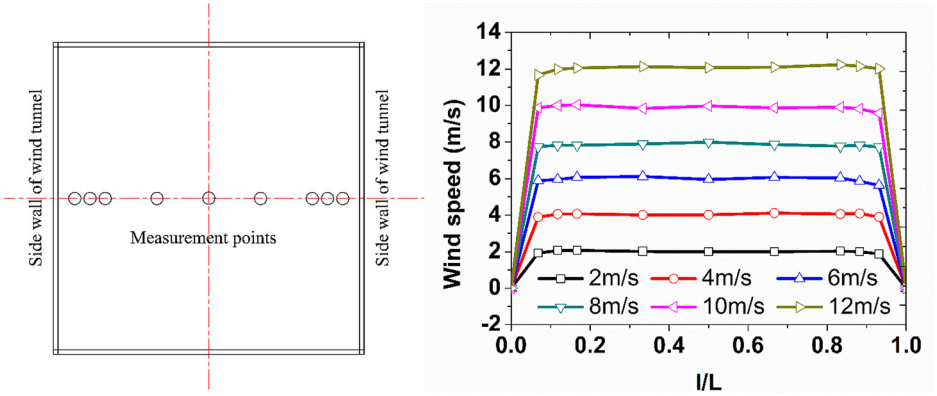

FIG. 2. Wind speed distribution along the central line of the testing section.

two transparent windows at the tunnel side through which the running conditions of the tested rotor can be observed.

A variable-frequency controller is provided to drive the fan and regulate the wind speed within the range of 0–30 m/s. In order to make sure that the rotor is tested by the uniform incoming air flow, the rotor is placed at the central area of the test section of the wind tunnel. The length of the test section is 2 m. In the test section, we set nine measurement points in the middle cross section (left of Figure 2) when wind speed varied from 2 m/s to 12 m/s using a TSI hot wire anemometer with 0.01 m/s accuracy. We placed the TSI hot wire anemometer at the appointed nine points to record the wind speed data lasting for 1 min. We averaged the recorded wind speed data to gain the average wind speed at each point. Figure 2 (right) displays the wind distribution at nine points when the wind speed varied from 2 m/s to 12 m/s. Although a small decay of wind speed was found at points which were close to the wall of the wind tunnel, the wind speed distribution was fairly uniform along the central line of the tunnel when the wind speed varied from 2 m/s to 12 m/s. The recorded wind speed data at the central point of the test section are also used to calculate the standard deviation of the wind speed (Table I). The standard deviation indicates the uniformity of the wind speed at one point. It is found that the standard deviation of the wind speed ranged from 0.32% to 0.47%. This uniform wind speed distribution and small standard deviation at the test section provided a desirable testing condition for the Savonius rotor.

B. Test rig and procedure

Considering the axis orientation, there are two types of test rigs that are the horizontal test rig[26,27] and the vertical test rig.[12,28,29] Theoretically, these two test rig types can satisfy the testing requirements for any test condition. At the very beginning, we adopted the horizontal test rig as shown on the right side of Figure 3 and placed most part of the test rig outside the wind tunnel to attain and maintain a small blockage ratio. However, as the test went on, it was discovered that the shaft had to be rigid enough to sustain the unbalance force caused by the rotating rotors. As tiny unbalance of the rotating system at high rotational speed will generate astonishingly excessive stress, vibration and noise, it became more and more difficult to control the axiality of each component in the test. In addition, we found that the horizontal test rig (Figure 3) is receivable for the condition in which the test rig is erected completely outside the wind tunnel or the size of the wind tunnel is large enough. Based on our testing experience, the configuration of the Savonius

TABLE I. Standard deviation of wind speed at central point of testing section.

Wind speed	4	6	8	10	12
Standard deviation of wind speed	0.004725	0.00493	0.003752	0.003218	0.003391

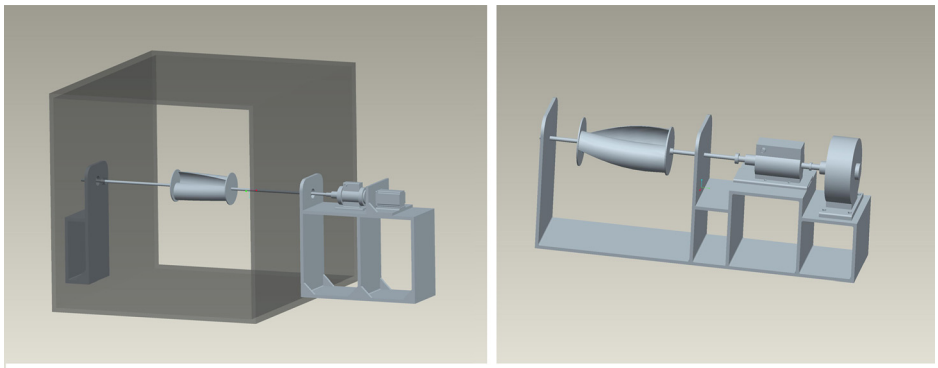

FIG. 3. The horizontal test rig.

rotor is naturally unbalance at no-zero azimuth angel for the horizontal test rig when measuring the static torque coefficient. It means that the Savonius rotor will return from the no-zero azimuth angle state to the zero azimuth angle state without any load in the horizontal test rig. But this unbalance can be easily eliminated in the vertical test rig.

Out of consideration for those problems, a vertical test rig was built showed in Figure 4 (left). This vertical test rig was manufactured using the computerized numerical control (CNC) machine. To attain easy manufacturing and high mechanical strength, aluminum alloy was chosen as the material for the test rig. Each component of the test rig was built to a tolerance of 0.01 mm to ensure the axiality. Components involved in this test included bearings, bearing holds, magnetic bearing, couplings, torque meters, flyer wheel, and motor. All these components are presented on the left side of Figure 4. The basic function of the magnetic bearing was to reduce the transmission of vibration caused by rotating unbalance and minimize the usage of the mechanical bearing in order to reduce the friction force. In the same time, all mechanical bearings were washed using the gasoline to remove the bearing grease which might increase the friction. Under the magnetic bearing, there is a torque meter having a measuring range of 0–2 Nm and an accuracy up to 0.01 Nm. This torque meter will record torque signals and rotational speed signals simultaneously and transmit them to a computer through the RS-232 port. A homemade software is programmed to process those signals and write them into a related file. At the end of the test rig, a motor is provided to drive the torque meter, magnetic bearing, and tested rotor by way of the motor controller and keep the rotor rotate at a specified rotational speed or a specified tip speed ratio (TSR). To ensure minimum blockage, only one

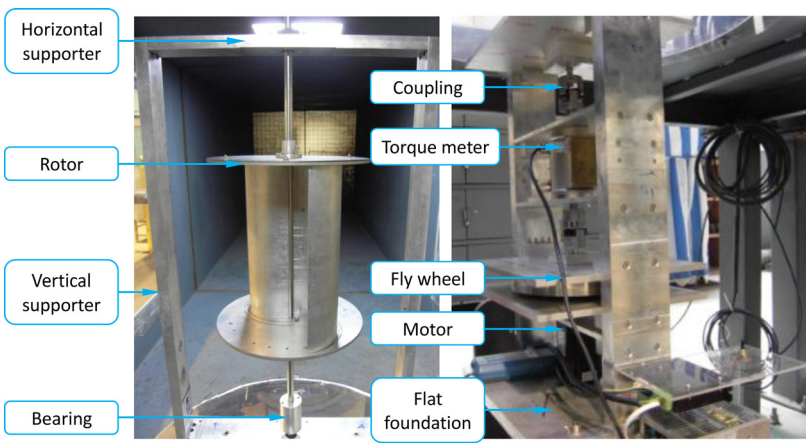

FIG. 4. The vertical test rig.

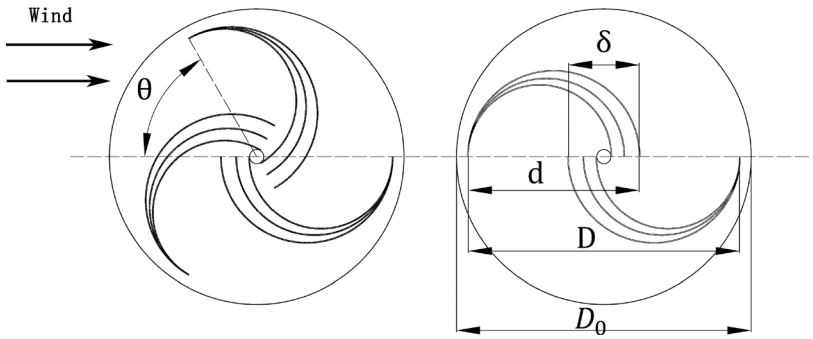

FIG. 5. Two and three blades Savonius rotor.

horizontal and two vertical supports are placed inside the wind tunnel. A flat foundation outside the wind tunnel holds the rest part of the test rig (right side of Figure 4).

In this paper, a frequency controller was used to regulate the wind speed with a fixed value. And we used a motor controller to adjust the rotational speed of the motor to gain different TSRs. TSR is obtained by the following equation:

$$\mathrm{TSR} = \frac{\omega \mathrm{r}}{V}, \tag{1}$$

where ω is the rotational speed of the Savonius rotor, r is the radius of the Savonius rotor, and V is the speed of wind pass through the wind tunnel.

The instantaneous dynamic torque was recorded lasting for 3-min at fixed wind speed and fixed TSR value, and recorded values were then averaged to gain the average dynamic torque coefficient (C_T). The product of C_T and TSR was the power coefficient (C_P). The instantaneous static torque was recorded for 3 min at a fixed wind speed and a fixed azimuth angle. The average static torque meter (AC_{TS}) was gained by averaging the instantaneous static torque. The next AC_{TS} testing is carried out after an interval of 5°.

C. Tested models

Main components of the Savonius rotor include two end-plates, two or three blades, and one shaft.[30] Generally, the C_P of the rotor with endplates is higher than that of the rotor without the endplates.[15] In the test, most of the components except the shaft were fabricated with aluminum alloy (6061-T6). Two or three semicircular slots and one circular hole were formed using the wire-electrode cutting machine to accommodate, respectively, the semicircular aluminum blades and shaft. Blades were rolled up with a cylinder inside. This cylinder had the same diameter as the designed blade. Based on other researches, the optimal size of endplate (D_0) is about 1.1 times the rotor diameter (D).[31] As D_0 is 250 mm, D should be 227.27 mm. This value is then rounded up to 230 mm to facilitate the measurement. In order to keep D constant, the blade diameter (d) is adjusted according to different GRs. The diameter of the shaft, which is denoted as a, is 12 mm to maintain the stiffness, and the height (H) of the rotor is 272 mm; thus, the aspect ratio of the rotor is 1.088.

According to previous researches, the best GR of Savonius rotor without shaft is 1/6 or ranges from 0.20 to 0.30.[17,31] Whether the shaft exists or not is likely to alter this range. Thus, three GRs different from those in other researches were selected in this paper, and were 0, 1/6, and 1/3. The equation for GR is

$$\mathrm{GR} = \frac{\delta - \mathrm{a}}{d}, \tag{2}$$

TABLE II. Detailed geometry information of two- and three-blade Savonius rotors (in mm).

Blade number	Model designation	Blade diameter	Gap between two blades	GR	Rotor diameter	Rotor height
2	S1B2GR0	121	12	0	230	270
	S1B2GR1/6	132	34	1/6	230	270
	S1B2GR1/3	145	60	1/3	230	270
3	S1B3GR0	121	12	0	230	270
	S1B3GR1/6	132	34	1/6	230	270
	S1B3GR1/3	145	60	1/3	230	270

where a is the diameter of the shaft, d is the blade diameter, and δ is the gap between two blades. Unlike equations in other researches, this equation takes into account the effect of the shaft. All definitions of design parameters for two- and three-blades rotors can be found in Figure 5. Different from the test conducted by Blackwell *et al.*,[21] the blade profile of the three-blade rotor in this paper was constructed with a 180° arc, instead of a 150° arc, to facilitate manufacturing and fabrication. Meanwhile, Table II summaries the value of each design parameter and the testing designation of each model.

III. WIND TUNNEL BLOCKAGE CORRECTION AND MEASUREMENT UNCERTAINTY

A. Blockage correction

Considering the increase of local wind speed in the test section, the blockage of the Savonius should be considered.[32] Two wind tunnel blockage correction methods are widely used, i.e., the Pope and Harper[33] and the Maskell[34] methods. Generally, the wind tunnel correction is to ascertain the ε and m factor for the Pope's method and Maskell method, respectively. However, it is very difficult to determine these two factors for an unusual shape, such as the Savonius rotor. Alexander[35,36] extended the Maskell's method to make it suitable for the wind tunnel test of the Savonius rotor.

The Alexander's correction method is given as follows:

$$\text{Ø} = \frac{C_{Du}}{C_{D\infty}} = \frac{q_c}{q_u} = \frac{v_c^2}{v_u^2} = \frac{1}{1 - m(S/C)}, \tag{3}$$

where m is determined in the wind tunnel test; v_c is the corrected wind speed; v_u is undisturbed wind speed; S is the model frontal area of the test model and rig; and C is the frontal area of the test section.

Figure 6 is the Alexander correction for Savonius rotor tested in the wind tunnel. In addition, Alexander's method can get accurate correction results even when the S/C value reaches up to 0.334. In this test, the swept area of the tested rotor was 0.06256 m^2 and the frontal area of related supporting components was 0.004 m^2. Hence, S was equal to 0.06656 m^2 and the frontal area of the test section was 1.1025. So, the S/C value of this test was about 0.060372 which is far less than the value of 0.334. All the experimental data in this paper were corrected using the Alexander method. The RN is calculated using the following equation:

$$RN = VD/\vartheta, \tag{4}$$

where V is wind speed. D is the diameter of the rotor and ϑ is Kinematic viscosity.

B. Measurement uncertainty

The standard deviation was used to estimate the experimental uncertainty associated with the wind velocity, torque, measured RPM, and tip speed ratio and the following equation was used to calculate the standard deviation of variants mentioned above

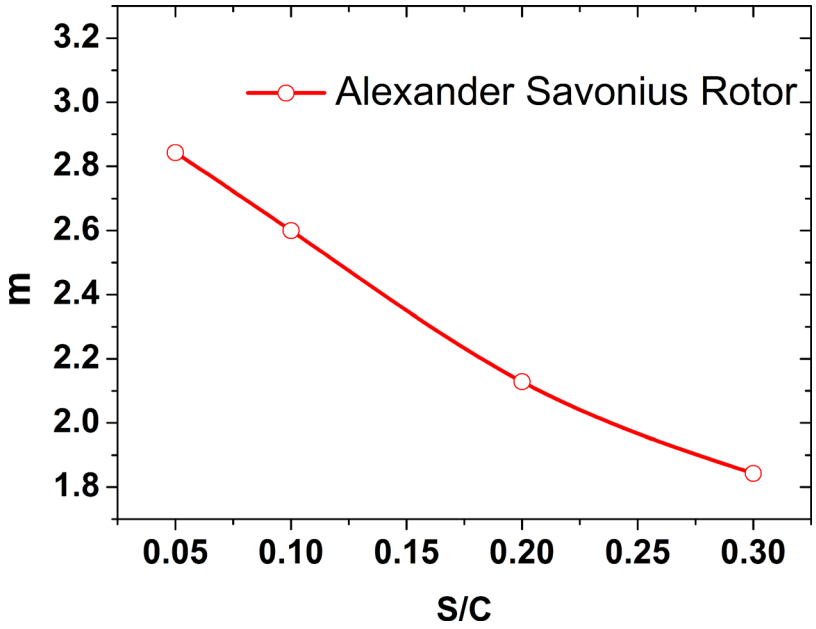

FIG. 6. The Alexander blockage correction method.

$$E_{st} = \sqrt{\frac{(x_1 - x_{mean})^2 + (x_2 - x_{mean})^2 + \cdots + (x_n - x_{mean})^2}{n-1}}, \tag{5}$$

where x means the measured values and n means the total number of measurements. Some unforeseen results were repeated several times to minimize the measurement error. Table III shows the percentage of the measurement uncertainty of each variant. The uncertainty of the wind velocity, torque, RPM, and TSR ranged, respectively, from 1.8% to 3.61%.

IV. RESULTS

In this section, the effects of wind speed, GR and Blade number on AC_{TS} and C_P were discussed in detail. AC_{TS} was gained at various azimuth angles ($\theta = 0°$–$180°$ with steps of $5°$) in respect of the oncoming wind. The definition of θ can be found in Figure 5. AC_{TS}, C_T, and C_P are expressed by the following equations, respectively,

$$AC_{TS} = \frac{TS}{0.5\rho AV^2R}, \tag{6}$$

$$C_T = \frac{T}{0.5\rho AV^2R}, \tag{7}$$

TABLE III. Uncertainty percentage of each variant.

Variant	Uncertainty (%)
Wind velocity	1.8
Measured torque	3.4
Measured RPM	3.2
Measured TSR	3.61

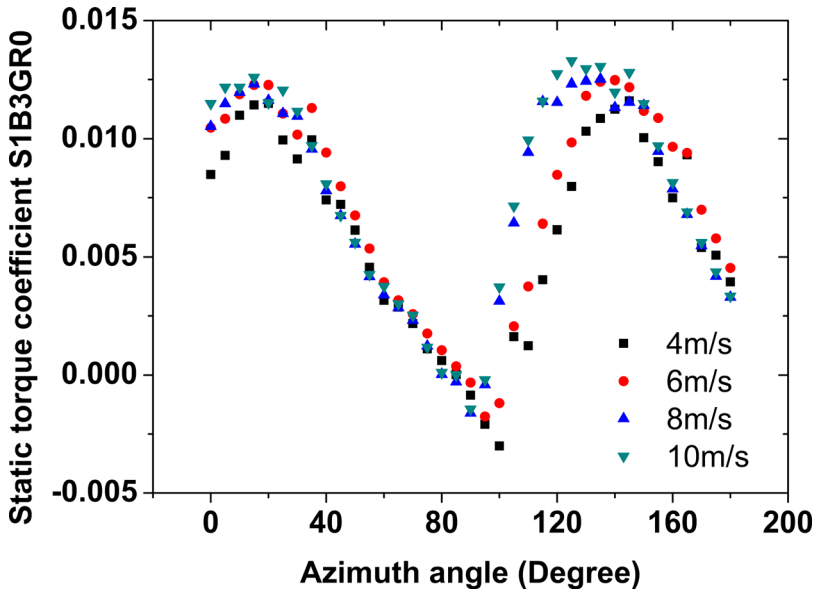

FIG. 7. Wind speed effect on AC_{TS} of the Savonius rotor with three blades.

$$C_P = C_T * \mathrm{TSR}, \tag{8}$$

where V (m/s) is the oncoming wind speed; A (m^2) is the swept area of the Savonius rotor; TS (Nm) is the measured static torque; R (m) is the radius of the Savonius rotor; T (Nm) is the measured dynamic torque; TSR is the tip speed ratio; ρ (kg/m^3) is the density of wind; AC_{TS} is the average static torque coefficient; C_T is the dynamic torque coefficient; and C_P is the power coefficient. T is gained at various TSRs to calculate the related C_T.

A. Static torque coefficient

1. Wind speed effect on AC_{TS}

Figure 7 presents the effect of wind speed on AC_{TS} of the Savonius rotor with three blades at four different wind speed when GR = 0. In this three-blade configuration, three peaks appeared within the whole azimuth angle range (0°–360°). In theory, the AC_{TS} curve over the range of 0°–120° is sufficient to describe the AC_{TS} curve over the whole azimuth angle range. In order to compare the three-blade rotor with the two-blade rotor, the azimuth angle range in this paper varied from 0° to 180°. Thus, the AC_{TS} curve of a three-blade rotor had two peaks within the 0°–180° azimuth angle range.

It is known from the figure that the AC_{TS} curve at wind speed 4 m/s is close to the AC_{TS} curve at wind speed 6 m/s; that the AC_{TS} curve at wind speed 8 m/s almost coincides with the AC_{TS} curve at wind speed 10 m/s; and that AC_{TS} curves at 4 m/s and 6 m/s are lower than AC_{TS} curves at 8 m/s and 10 m/s. Every case has the same variation pattern with different wind velocities, and which is agreed with the Blackwell's conclusion, that the same change trend of static torque can be obtained under different RN. But with the increase of RN, the difference between the peak and valley value decreased. A relatively large distinction between AC_{TS} curves at 6 m/s and 8 m/s within azimuth angle ranges of 0°–20° and 90°–120° was observed, which might be caused by the initial friction force and specific separation patterns for different wind speeds. It can also be indicated that the wind speed had a slight effect on AC_{TS} of the Savosnius rotor and that this effect varied regionally. Peaks of four AC_{TS} curves at different wind speeds were fairly close to each other in terms of location and amplitude and this characteristic can be found in Table IV that presents the AC_{TSmax} and AC_{TSmin} with respect to the

TABLE IV. The AC_{TSmax} and AC_{TSmin} of the rotor with three blades.

	4 m/s	6 m/s	8 m/s	10 m/s
AC_{TSmax}	0.0115	0.01228	0.01233	0.01259
Azimuth angle (C_{Pmax})	20	20	15	15
AC_{TSmin}	−0.00301	−0.00119	−0.00161	−0.00144
Azimuth angle (C_{Pmin})	100	100	90	90

related azimuth angle. Due this independence, the GR and Blade Number (BN) effects were discussed at wind speed of 8 m/s.

2. GR effect

Figure 8 shows AC_{TS} varying with the azimuth angle for two-blade Savonius rotor at different gap ratios when the wind speed is 8 m/s. It is found that there were some azimuth positions where the AC_{TS} was negative at three gap ratios within azimuth angle ranges of 130°–180° (when gap ratio = 0), 155°–175° (when GR = 1/6), and 135°–160° (when gap ratio = 1/3).

The two-blade rotor with zero GR had the widest negative range, indicating that with the increase of GR, the negative azimuth angle decreased. An interesting finding is that negative azimuth angle range moved forward as GR increased. In addition, a significant improvement of AC_{TS} was found for rotor (GR = 1/3) within azimuth angle ranges of 90°–125° and 165°–180°, indicating that the existence of the gap will generally increase the AC_{TS} of the Savonius rotor and improve the rotor's starting ability. The reason behind this phenomenon is that the wind flow passed through the gap and imposed an additional force on the returning blade.

Compared with the results of Blackwell, the same conclusion was that the AC_{TS} curve moved up with the increase of GR and all the curves have the same rules. Blackwell gained the negative static torque only at the zero GR and the rest cases with different GR all had the positive static torque. However, in our testing, the negative static torque can be obtained in every

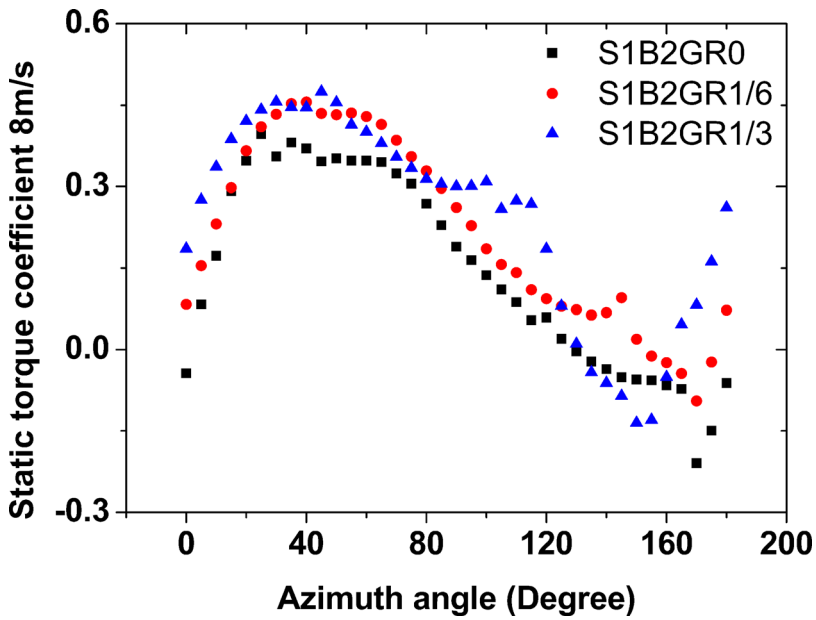

FIG. 8. The effect of GR on AC_{TS} for rotor with two blades (8 m/s).

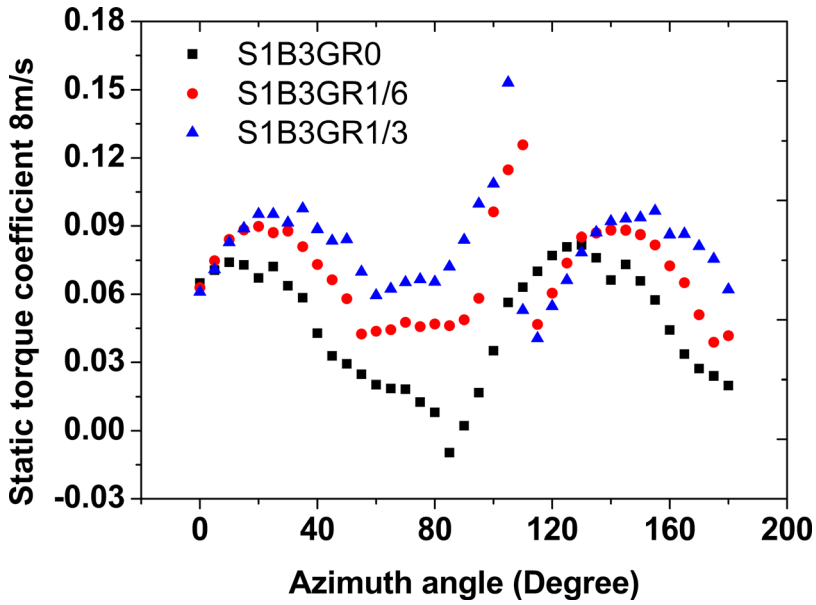

FIG. 9. The effect of GR on the static torque coefficient for rotor with three blades.

GR condition, not only zero GR. And the peak of AC_{TS} is lower than Blackwell's result, which is 0.7 and ours is 0.55.

The effect of GR on AC_{TS} of the rotor with three blades at the wind speed of 8 m/s is shown in Figure 9. Generally, increasing GR (from 0.0 to 1/6 and 1/3) for the rotor with three blades will increase the value of AC_{TS} and smooth the AC_{TS} curve, which is similar with the Blackwell's curves. However, there is an obvious step at azimuth angle 120° in our data, which is absent in Blackwell's curve. Except for the case where GR is zero, AC_{TS} was positive for all azimuth angles. The only negative AC_{TS} was found at azimuth angle 85° for the three-blade rotor with zero GR, suggesting that the three-blade rotor with zero GR can be started at almost any azimuth angle without friction force or load. While all the data of static torque in Blackwell's paper was positive. It is also found that AC_{TSmin} of the three-blade rotor with 1/6 and 1/3 GRs was about 0.03, meaning that the three-blade rotor with 1/6 and 1/3 GRs can be started to run at any azimuth angle and be used to assist the startup of the Darrieus rotor. The rotor with a 1/3 GR had the highest AC_{TSmax} (0.15).

3. Blade number effect

The effect of blade number was investigated for rotors with two and three blades at wind speed of 8 m/s. Figure 10 shows the comparison of AC_{TS} values for the zone spanning from 0 to 180. From this figure, it can be clearly seen that the maximum AC_{TS} values of rotors with two blades were much higher than the maximum AC_{TS} value of rotors with three blades, especially within the azimuth angle range of 0°–110°. However, rotors with two-blade exhibited a very low AC_{TS} within the range of 112°–180°. For the three-blade configuration, there was almost no azimuth angle where the static torque coefficient was negative. Moreover, the three-blade configuration exhibited a smaller variation in AC_{TS} than the two-blade configuration. AC_{TS} values of the three-blade configuration were normally within the range of 0.03–0.10 for one cycle and were smaller than those of the two-blade configuration (AC_{TS} values of the two-blade configuration were within the range of −0.25–0.50), all indicating that the three-blade rotor has a good starting ability than the two-blade rotor in terms of smooth curve and positive AC_{TS}. Overall, increasing the blade number could smoothen the variation of AC_{TS} curves and eliminate AC_{TS}'s negative range. The reason behind this phenomenon is that the total drive

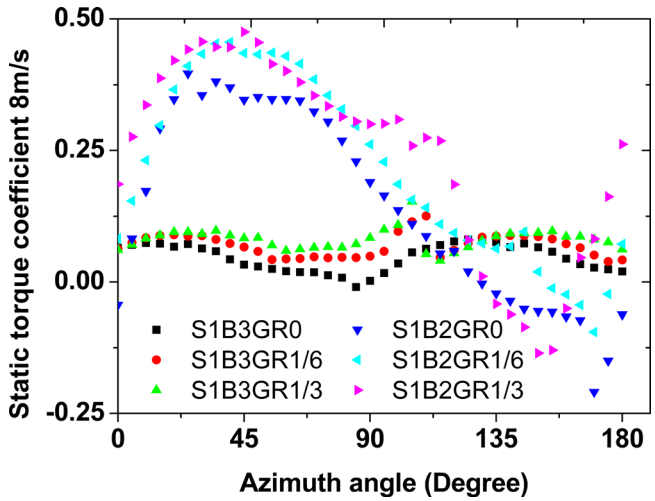

FIG. 10. The effect of blade number on the static torque coefficient.

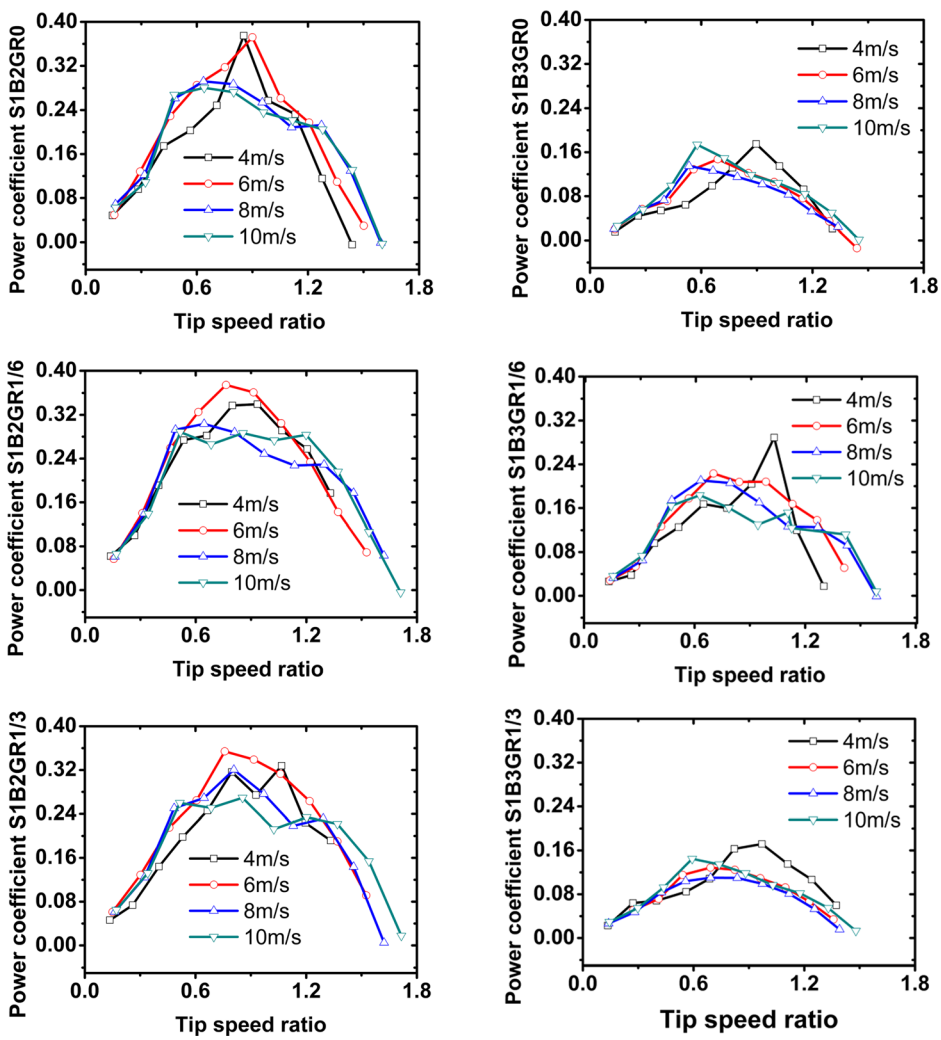

FIG. 11. The Wind speed effect on the power coefficient of the Savonius rotor.

TABLE V. Relationship between wind speed and RN.

RN and wind speed	
Wind speed	RN
4 m/s	62 162.16
6 m/s	93 243.24
8 m/s	124 324.3
10 m/s	155 405.4

force is the superposition of drive force on each blade; as each blade has one AC_{TS} curve and the phase shift angle of AC_{TS} curve between blades becomes smaller, the superposition of each blade's AC_{TS} curve will smooth the total AC_{TS} curve.

B. Power coefficient

1. Effects of wind speed and blade number

The effects of wind speed and blade number are examined in Figure 11 for both rotor types. The relationship between the RN and wind speed is shown in Table V, where the wind speed effect is displayed for each tested rotor. Generally, there was a slight improvement in performance as wind speed increased from 4 m/s to 6 m/s, and the lower wind speed data performed better within the range from 8 m/s to 10 m/s for the two-blade Savonius rotor. It is speculated that the lower RN, about 10^4 orders, has the better performance. While in Blackwell's plots, there were curves only for high RN, about 10^5 orders, and the results showed slightly different. For the three-blade Savonius rotor, the scenario was different whereas wind speed increased from 4 m/s to 6 m/s, the power coefficient decreased slightly, and the higher wind speed data performed better within the range of 6 m/s–10 m/s. Another finding is that with the increase of wind speed, the C_P curve became flat at the maximum C_P area. And it cannot be found so obviously different in Blackwell's results.

Figure 11 also compares the performance between typical two- and three-blade configurations. From the perspective of performance, the two-blade configuration was superior in most respects. The maximum power coefficient of the two-blade configuration was approximately 1.5 times that of the three-blade configuration. The reason for the low power output of the three-blade rotor may be due to the superposition of the instantaneous C_P of three blades. Another finding is that the working TSR range of the two-blade rotor was wider than that of the three-blade rotor in general. The maximum TSR value was about 1.7 for the two-blade rotor, but only 1.5 for the three-blade rotor. The rotor with a wider TSR range can easily match with the generator's curve. At the position of the maximum C_P, the TSR decreased when the number of blades went from two to three. For the two-blade configuration, the optimum speed ratio was between 0.7 and 0.8, which, however, was 0.5–0.6 for the three-blade configuration. This conclusion is the same with those obtained by researches without central shaft, suggesting that rotors with three blades had a stronger drag property than rotors with two blades. Thus, rotors with three blades had a better starting ability and weaker power output when compared to rotors with two blades.

2. GR effect

The effect of GR on rotor performance for two-blade configuration is presented in Figure 12 where the performance was evaluated at three GRs ranging from 0.0 to 1/6 and 1/3 as the wind speed increased from 4 m/s to 10 m/s. The 1/6 GR test data in Figure 12 exhibited the attainment of super performance for all wind speed. Both larger and smaller gaps showed a decrease in performance, and the distribution curve was Parabolic. Optimum TSR was within the 0.8–1.0 range when wind speed = 4 m/s, and the maximum C_P was about 0.3. With the increase of the wind speed, the optimum TSR decreased, so did the maximum C_P. The maximum C_P attained 0.25 at

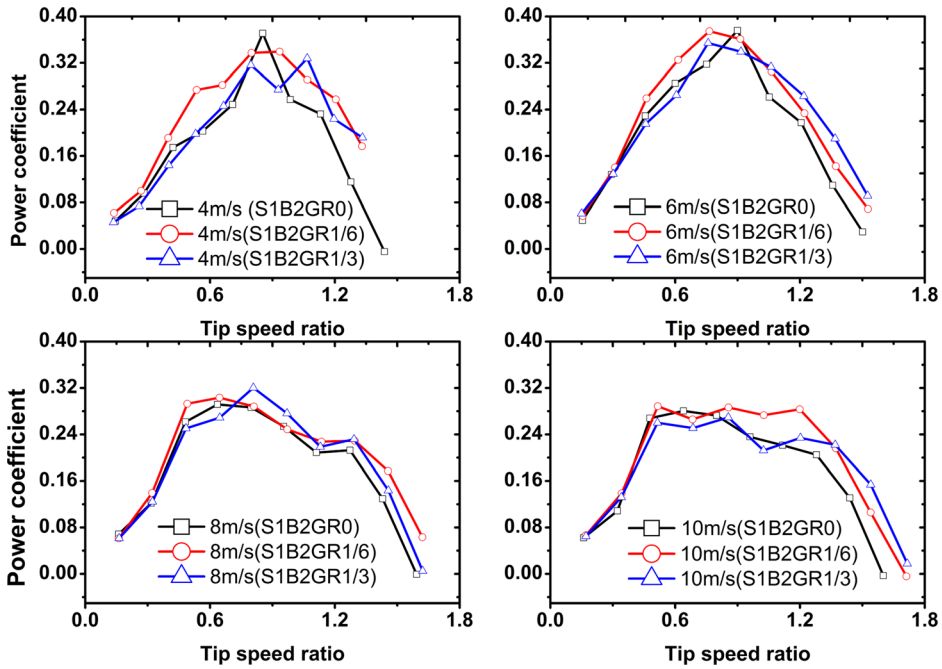

FIG. 12. GR effect on the power coefficient of the Savonius rotor (two-blade rotor).

the wind speed of 8 m/s when the optimum TSR ranged from 0.5 to 0.6. The curve had a quick spike before attaining the best TSR, and then dropped when climbing over the peak. At the wind speed of 10 m/s, there was an obvious flat area for TSR between 0.5 and 1.2, indicating that the high wind speed can provide a broader range of high power work and stable power output.

Figure 13 presents the effect of GR on rotor performance for three-blade configuration within the range from 0.0 to 1/6 and 1/3 GR as the wind speed increases from 4 m/s to 10 m/s. The 1/6 GR test data in Figure 13 also exhibited the attainment of super performance for all

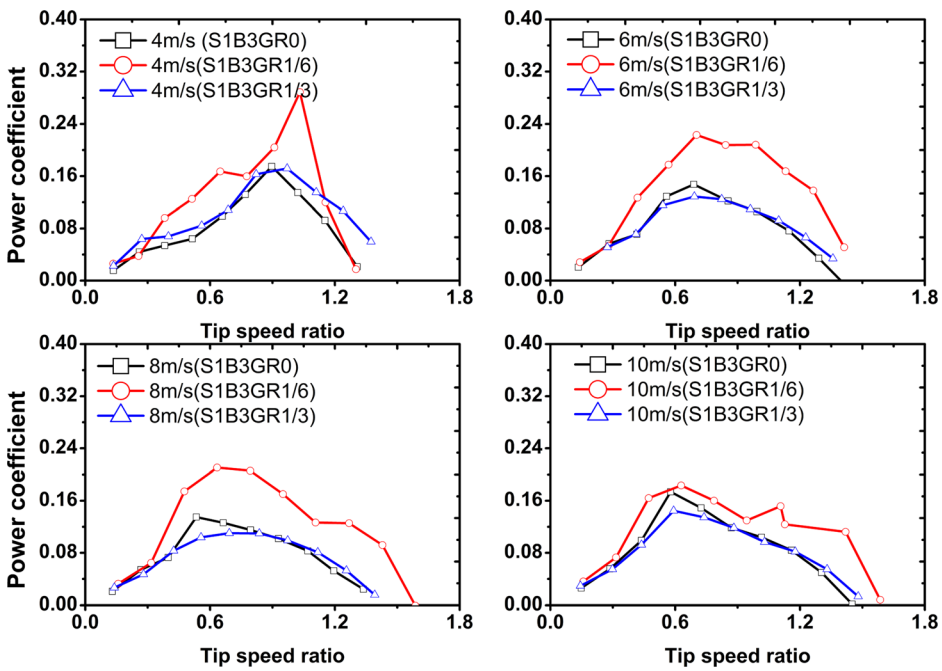

FIG. 13. GR effect on rotor performance (three-blade rotor).

wind velocities. Both larger and smaller gaps showed a decrease in performance, which is agreed with the conclusion of Blackwell. The distribution curve was also Parabolic. The performance difference became most noticeable when the wind speed was 6 m/s and 8 m/s. The optimum speed ratio was within the 0.8–1.0 range when wind speed = 4 m/s, and the maximum C_P was about 0.25. With the increase of the wind speed, the optimum TSR decreased, so did the maximum C_P. The maximum C_P was 0.20 within the 0.6–0.8 optimum TSR range when wind speed = 8 m/s. The curve had a quick spike before attaining the best TSR, and then dropped when climbing over the peak. At the wind speed of 10 m/s, the maximum value was reduced to about 0.16 within the same optimum TSR range.

V. CONCLUSION

A detailed experimental test of two- and three-blade rotors with central shaft was conducted at different wind speeds to offer some directions for the selection of Savonius rotors.

By exploring and discussing the effects of wind speed, GR, and BN on AC_{TS}, it is found that wind speed has a small effect on AC_{TS} curves. Test results suggest that with the increase of GR, the azimuth angle range of negative AC_{TS} decreases, and the negative azimuth angle range moves forward as GR increases; and that increasing BN from two to three, AC_{TS} curves become smooth and less varied and the negative range of AC_{TS} is almost eliminated.

In terms of the effects of wind speed, GR, and BN on C_P, it is known from the 1/6 GR test data that the best performance is observed on rotors with two and three blades. Moreover, the two-blade configuration is superior than the three-blade configuration. The maximum power coefficient of the two-blade configuration is approximately 1.5 times that of the three-blade configuration. Another finding is that with the increase of wind speed, the C_P curve becomes flat at the maximum C_P area.

ACKNOWLEDGMENTS

The work described in this paper was supported by the Shanghai Pujiang Program (Grant No. 15PJ1406200) and Shanghai Outstanding Talents Support Program (Grant No. 5113301101). Appreciation is also given to the Dean Reserve funding of The Hong Kong Polytechnic University (1-ZV3W).

[1]D. W. Wekesa *et al.*, "A numerical analysis of unsteady inflow wind for site specific vertical axis wind turbine: A case study for Marsabit and Garissa in Kenya," Renewable Energy **76**, 648–661 (2015).
[2]B. K. Kirke, "Evaluation of self-starting vertical axis wind turbines for stand-alone applications," in *School of Engineering* (Griffith University, 1998).
[3]A. Peacock *et al.*, "Micro wind turbines in the UK domestic sector," Energy Build. **40**(7), 1324–1333 (2008).
[4]W. El-Askary *et al.*, "Harvesting wind energy for improving performance of Savonius rotor," J. Wind Eng. Ind. Aerodyn. **139**, 8–15 (2015).
[5]M. Tartuferi *et al.*, "Enhancement of Savonius wind rotor aerodynamic performance: A computational study of new blade shapes and curtain systems," Energy **79**, 371–384 (2015).
[6]Z. Driss *et al.*, "Numerical simulation and experimental validation of the turbulent flow around a small incurved Savonius wind rotor," Energy **74**, 506–517 (2014).
[7]N. Sarma, A. Biswas, and R. Misra, "Experimental and computational evaluation of Savonius hydrokinetic turbine for low velocity condition with comparison to Savonius wind turbine at the same input power," Energy Convers. Manage. **83**, 88–98 (2014).
[8]M. Kamoji, S. Kedare, and S. Prabhu, "Performance tests on helical Savonius rotors," Renewable Energy **34**(3), 521–529 (2009).
[9]M. Kamoji, S. Kedare, and S. Prabhu, "Experimental investigations on single stage modified Savonius rotor," Appl. Energy **86**(7–8), 1064–1073 (2009).
[10]M. Mohamed *et al.*, "Optimal blade shape of a modified Savonius turbine using an obstacle shielding the returning blade," Energy Convers. Manage. **52**(1), 236–242 (2011).
[11]P. Reupke and S. D. Probert, "Slatted-blade Savonius wind-rotors," Appl. Energy **40**, 65–75 (1991).
[12]P. Ghosh *et al.*, "Model testing of single-and three-stage modified Savonius rotors and viability study of modified savonius pump rotor systems," Int. J. Green Energy **6**(1), 22–41 (2009).
[13]J. Chen *et al.*, "Influence of phase-shift and overlap ratio on savonius wind turbine's performance," J. Sol. Energy Eng. **134**, 011016 (2012).
[14]U. Saha, S. Thotla, and D. Maity, "Optimum design configuration of Savonius rotor through wind tunnel experiments," J. Wind Eng. Ind. Aerodyn. **96**(8), 1359–1375 (2008).
[15]B. D. Plourde *et al.*, "An experimental investigation of a large, vertical-axis wind turbine: Effects of venting and capping," Wind Eng. **35**, 213–222 (2011).

[16]S. Sivasegaram, "Wind tunnel tests on slow-running vertical-axis wind-rotors," Proc. Indian Acad. Sci. **4**, 395–404 (1981).
[17]I. Ushiyama and H. Nagai, "Optimum design configurations and performance of Savonius rotors," Wind Eng. **12**(1), 59–75 (1988).
[18]I. Ushiyama, H. Nagai, and J. Shinoda, "Experimentally determining the optimum design configuration for Savonius rotors," Bull. JSME **29**(258), 4130–4138 (1986).
[19]B. Newman, "Measurements on Savonius rotor with variable gap," in Proceedings of the Sherbrook University Symposium on Wind Energy, Sherbrook, Canada (1974).
[20]M. Kamoji, S. Kedare, and S. Prabhu, "Experimental investigations on single stage, two stage and three stage conventional Savonius rotor," Int. J. Energy Res. **32**(10), 877–895 (2008).
[21]B. F. Blackwell *et al*., *Wind Tunnel Performance Data for Two-and Three-Bucket Savonius Rotors* (Sandia Laboratories, 1977).
[22]M. Q. Islam, M. N. Hasan, and S. Saha, "Experimental investigation of aerodynamic characteristics of two-, three- and four bladed S-shaped stationary Savonius rotors," in *Proceedings of the International Conference on Mechanical Engineering 2005 (ICME2005), 28–30 December 2005, Dhaka, Bangladesh* (ICME, 2005), paper ICME05-FL-23.
[23]A. Biswas, R. Gupta, and K. Sharma, "Experimental investigation of overlap and blockage effects on three-bucket Savonius rotors," Wind Eng. **31**(5), 363–368 (2007).
[24]K. N. Morshed *et al*., "Wind tunnel testing and numerical simulation on aerodynamic performance of a three-bladed Savonius wind turbine," Int. J. Energy Environ. Eng. **4**(1), 18 (2013).
[25]T. Hayashi, Y. Li, and Y. Hara, "Wind tunnel tests on a different phase three-stage savonius rotor," JSME Int. J. Ser. B **48**(1), 9–16 (2005).
[26]S. Roy and U. K. Saha, "Wind tunnel experiments of a newly developed two-bladed Savonius-style wind turbine," Appl. Energy **137**, 117–125 (2015).
[27]M. Nakajima, S. Iio, and T. Ikeda, "Performance of Double-step Savonius Rotor for Environmentally Friendly Hydraulic Turbine," J. Fluid Sci. Technol. **3**(3), 410–419 (2008).
[28]J. L. Menet, "A double-step Savonius rotor for local production of electricity: A design study," Renewable Energy **29**(11), 1843–1862 (2004).
[29]U. Saha and M. J. Rajkumar, "On the performance analysis of Savonius rotor with twisted blades," Renewable Energy **31**(11), 1776–1788 (2006).
[30]J. P. Abraham *et al*., "Summary of Savonius wind turbine development and future applications for small-scale power generation," J. Renewable Sustainable Energy **4**(4), 042703 (2012).
[31]N. Fujisawa, "On the torque mechanism of Savonius rotors," J. Wind Eng. Ind. Aerodyn. **40**, 277–292 (1992).
[32]J. P. Abraham *et al*., "Numerical simulation of fluid flow around a vertical-axis turbine," J. Renewable Sustainable Energy **3**(3), 033109 (2011).
[33]A. Pope and J. Harper, *Low Speed Wind Tunnel Testing* (John Wiley & Sons, New York, 1966).
[34]E. Maskell, "A theory of the blockage effects on bluff bodies and stalled wings in a closed wind tunnel," Report No. ARC R&M 3400, London, 1965.
[35]A. Alexander and B. Holownia, "Wind tunnel tests on a Savonius rotor," J. Wind Eng. Ind. Aerodyn. **3**(4), 343–351 (1978).
[36]A. Alexander, "Wind tunnel corrections for Savonius rotors," NASA STI/Recon Technical Report A No. 79, p. 40127.